

# Thermal structure of the Pacific lithosphere with reheating in the Central Pacific

Michael H. Ritzwoller, Nikolai M. Shapiro, & Shi-Jie Zhong

*Department of Physics, University of Colorado at Boulder, Boulder, CO 80309-0390 USA*

**A brief summary paragraph will go here.....**

Plate tectonics is the surface manifestation of thermal convection in the earth's mantle, which is expressed most simply in oceanic plates where a thermal boundary layer or "lithosphere" forms as the plate cools conductively during its journey away from mid-ocean ridges<sup>1-3</sup>. Few observables directly constrain the thermal state of the oceanic lithosphere or the "asthenosphere" that lies beneath it. Seafloor topography and heat flow<sup>4-6</sup> have been most commonly used to infer oceanic mantle temperatures as these surface observables reflect the average temperature and the temperature gradient in the uppermost mantle. The lithosphere is believed to cool with age because of the deepening of the sea-floor and the reduction in heat flow away from the mid-ocean ridges, but these trends cease and topography becomes much more erratic by about 80 Ma. This has led to a variety of hypotheses on the cause or causes of the reheating of old oceanic lithosphere, most consider convective processes which may be confined to the upper mantle (e.g., small-scale convection (SSC) directly beneath the lithosphere<sup>7-9</sup> or larger scale convection across the entire upper mantle<sup>10</sup>) or which may extend considerably deeper into the lower mantle (e.g. hot spot plumes<sup>11</sup> or larger scale limbs of global convection possibly associated with superswells<sup>12-13</sup>). Near surface structures, such as the accumulation of sediments<sup>14</sup>, the distribution of hot spots<sup>15</sup>, the formation of volcanic edifices<sup>16</sup>, and associated crustal thickening<sup>17</sup>, however, obscure the interpretation of surface observables alone. Within this context, the more direct probe of mantle structures provided by seismic waves<sup>13,18-20</sup>, which are less sensitive to the obscuring effects of surficial structures, is needed but the application of seismic models to lithospheric geothermometry has been limited in the past due to substantial uncertainties in the conversion from seismic velocities to temperatures and by poor station coverage across the Pacific seafloor that has limited both lateral and vertical resolution. Both issues have been increasingly ameliorated in recent years due to the growth of the global seismic network and advances in thermoelasticity<sup>21</sup>.

Seismic surface waves provide particularly uniform coverage of the Pacific lithosphere. The surface waves that emanate from earthquakes around the Pacific are observed at both continental and ocean island stations, and now densely sample much of the Pacific basin. Observations of surface wave dispersion strongly constrain shear velocities which are related to temperatures in the uppermost mantle<sup>21</sup>. Using information about surface wave dispersion across the Pacific we estimated

a radially anisotropic (transverse isotropy with a radial symmetry axis) three dimensional (3-D) tomographic model of shear-wave velocity in the Earth’s upper mantle by a Monte-Carlo method<sup>22</sup> using both a seismic parameterization and a temperature parameterization which is based on a simple thermal model of the oceanic lithosphere and asthenosphere<sup>23</sup>. Inferences are similar using both parameterizations, but Figures 1-4a present results only from the temperature parameterization. With the temperature parameterization, there are two principal mantle unknowns. The first unknown is the “apparent thermal age”,  $\tau$ , of the lithosphere which is the age at which a conductively cooling half-space would match the observed lithospheric temperature structure. The second unknown is the “potential temperature”,  $T_p$ , of the asthenosphere which is the upward continuation to the surface of asthenospheric temperatures following the mantle adiabatic gradient. The motivation of the Monte-Carlo inversion is to estimate a range of seismic models and temperature models at each depth (e.g., Figs. 1c-1f) so that only features that appear in every member of the ensemble of acceptable models are interpreted. We refer to these features as “persistent”.

Figures 2a and 2b present the 3-D shear-velocity model at a depth of 100 km in the uppermost mantle. The general increase in shear-wave speed toward the western Pacific, as seen in Figure 2a, is consistent with the prediction for a diffusively cooling half-space (Half-Space Cooling or HSC model<sup>2,3</sup>). In fact, as Figure 2c shows, until about 70 Ma shear velocities at 100 km depth are, on average, in remarkable agreement with the predictions from the HSC model. A systematic deviation from the HSC model, however, appears in the Central Pacific at lithospheric ages that range from about 70 Ma to somewhat more than 100 Ma (Figure 2b, 2c). This deviation is manifest as a low speed anomaly running largely north-south across the Central Pacific, confined between the 70 Ma and 105 Ma age contours in Figure 2b. This reduction of shear-wave speed between 70 and 100 Ma is robust to data subsetting, to changes in the theory of wavefield sensitivity (ray versus diffraction tomography), to ad-hoc choices of damping, and is a persistent feature of the inversion. The deviation from the HSC model in this age range maximizes at about 100 km depth. At shallower and greater depths the pattern of the deviation is similar, but the amplitude reduces (Figure 2d, 2e).

The average shear velocity structure of the upper mantle beneath the Pacific, therefore, is predicted well by the HSC model up to a lithospheric age of about 70 Ma, but deviates from the HSC model at older ages. As seen in Figure 2f, the average Pacific isotachs deepen with lithospheric age, following the HSC model until about 70 Ma and then flatten until about 105 Ma, after which they deepen again. This deviation is shown in Figure 2g to set-on abruptly at about 70 Ma and maximizes in the deep lithosphere and shallow asthenosphere at depths between 70 km to 150 km. The approximately uniform deviation below 100 km seen in Figure 2g is caused by the fact that

the HSC model does not include adiabatic heating.

A similar evolutionary pattern is observed in temperature as Figure 3 shows. The thermal structure of the lithosphere is summarized efficiently by the apparent thermal age shown in Figure 3b. The apparent thermal age diverges systematically from the lithospheric age at about 70 Ma and remains depressed throughout the old Pacific. The average Pacific isotherms deepen with lithospheric age, as Figure 3d shows, displaying remarkable agreement with the HSC model until about 70 Ma where they flatten until about 100 Ma and deepen until about 135 Ma. This thermal pattern suggests two stages of lithospheric cooling from 0-70 Ma and again from 100-135 Ma bracketing an era of lithospheric reheating in the Central Pacific. The deficit in apparent lithospheric age that develops in the Central Pacific, referred to elsewhere as thermal resetting or extent of rejuvenation<sup>6</sup>, is seen in Figure 4a to grow until it reaches about 35 million years at a lithospheric age of 100 Ma. After this age, the age deficit remains approximately constant, on average, but becomes highly variable in the very old Pacific at lithospheric ages greater than about 135 Ma.

These findings indicate that, although there are regional variations, lithospheric age is a reliable predictor of the average thermal state of the lithosphere beneath the Pacific but the thermal evolution of the Pacific lithosphere deviates from a thermal model with diffusive cooling alone. The thermal structure of the Pacific lithosphere demonstrates a punctuated cooling history, cooling diffusively for the first 70 Ma after its creation. The cooling is arrested in the Central Pacific where the lithosphere is reheated, predominantly at ages between 70 - 100 Ma, and develops an average thermal resetting of about 35 Ma. At lithospheric ages from 100 Ma to about 135 Ma, the process or processes of reheating are substantially weaker than in the Central Pacific, and the lithosphere undergoes a second phase of diffusive cooling, on average. Beyond 135 Ma, the lithosphere may undergo a second reheating phase, but the thermal state of the very old lithosphere is highly variable and the statistics of inference are less favorable as the area covered by old lithosphere is smaller.

## Discussion

## Methods

### Construction of the 3-D shear velocity and temperature models

The inversion for a radially anisotropic 3-D tomographic model of shear-wave velocity and temperature is performed in two steps. In the first step Rayleigh and Love wave dispersion maps are constructed on a  $2^\circ \times 2^\circ$  grid globally. We compiled a large new data set of broad-band group velocity measurements<sup>24</sup> and produced Rayleigh and Love wave group velocity maps across the Pacific from 18 sec period to 200 sec for Rayleigh waves and from 20 sec to 150 sec for Love waves.

We also constructed phase velocity maps using measurements compiled at Harvard<sup>19</sup> and Utrecht<sup>25</sup> Universities from 40 sec to 150 sec period. The great length of most wavepaths across the Pacific necessitates considering the path-length dependent spatial sensitivity of the surface waves in order to model wave-front healing and associated diffraction effects<sup>26</sup>. The joint inversion of group and phase velocities provides better vertical resolution than either data type alone<sup>22</sup> providing unique information about the vertical variability of shear velocities in the uppermost mantle.

In the second step, values from the dispersion maps are used to construct a 3-D model on a  $2^\circ \times 2^\circ$  grid to 400 km depth based on two separate parameterizations: a seismic parameterization<sup>22</sup> and a temperature parameterization derived from a thermal model<sup>23</sup>. The seismic parameterization consists of 13 unknowns, seven in the crust and six in the mantle. The crust consists of three layers in which compressional ( $V_p$ ) and shear ( $V_s$ ) velocity are free variables as is crustal thickness; all seven crustal unknowns are perturbed from reference values taken from the model CRUST2.0 (G. Laske, personal communication, 2002). Isotropic mantle structure is parameterized with four radial cubic B-splines. The remaining two unknowns parameterize radial anisotropy (transverse isotropy with a radial symmetry axis). Because Rayleigh waves are predominantly sensitive to  $V_{sv}$  and Love waves to  $V_{sh}$ , we have constraints on only two of the five elastic moduli that describe a transversely isotropic medium. The two basis functions shown in Figure 1b are used to represent the split between  $V_{sh}$  and  $V_{sv}$  in the uppermost mantle to a depth of 220 km. The effective isotropic shear velocity,  $V_s$ , is defined as the average of the anisotropic velocities.

The inversion proceeds by a Monte-Carlo sampling that walks randomly through a subspace of model space defined by a-priori constraints and forms a Markov-chain similar to Brownian motion. At each point on the  $2^\circ \times 2^\circ$  grid, an ensemble of acceptable vertical profiles emerges such as those shown in Figure 1c-f. The bifurcation of the shear velocities in the uppermost mantle demonstrates the existence of radial anisotropy with a vertical structure that is free to vary across the Pacific<sup>19</sup>.

The temperature parameterization is based on a thermal model in which a thermally conductive layer (lithosphere) overlies a convective layer (asthenosphere) joined smoothly by a transition layer (Figure 1a). The temperature profile within the conductive layer is described by the half-space cooling solution given by equation  $T(z) = T_s + (T_m - T_s) \operatorname{erf}(z/2\sqrt{\kappa\tau})$ , where  $z$  is depth in the mantle,  $T_m$  is initial mantle temperature fixed at 1300°C,  $T_s = 0^\circ\text{C}$  is the surface temperature, thermal diffusivity  $\kappa = 1 \times 10^{-6} \text{ m}^2\text{s}^{-1}$ , and  $\tau$  is the ‘‘apparent thermal age’’ of the lithosphere. In the convective layer, the adiabatic temperature gradient  $D_a = 0.5^\circ\text{C}/\text{km}$  and the potential temperature  $T_p$  describe the thermal state of the asthenosphere.

Two mantle unknowns in the temperature parameterization specify the thermal state of the oceanic upper mantle:  $\tau$  in the lithosphere and  $T_p$  in the underlying asthenosphere. These two

unknowns replace the four  $B$ -splines in the seismic parameterization. The Monte-Carlo inversion with the temperature parameterization initiates in temperature space where a trial thermal model is constructed and converted to shear velocity in the mantle, then trial seismic crustal structures are introduced as well as mantle radial anisotropy similar to the generation of these features in the seismic parameterization. At each grid node, some temperature profiles are rejected entirely, but others fit the seismic data acceptably for an appropriate subset of seismic crustal models and models of radial anisotropy. These profiles then define the ensemble of acceptable profiles in temperature space and are also combined with the crustal and radial anisotropic models to define the ensemble of acceptable models in seismic velocity space. For both parameterizations, when a single model is needed, we use the middle of the ensemble of acceptable models.

### **Interconversion between temperature and shear velocity**

Interconversion between temperature and shear velocity is based on laboratory-measured thermoelastic properties of mantle minerals represented as partial derivatives of the elastic moduli with respect to temperature, pressure, and composition<sup>21</sup>. The compositional model for the oceanic upper mantle includes 75% Olivine, 21% Orthopyroxene, 3.5% Clinopyroxene, and 0.5% Spinel with an Iron-to-Magnesium ratio of 10%<sup>27</sup>. We compute shear velocity with the anelastic correction<sup>28</sup> from an anharmonic shear velocity,  $v_{anel}(P, T, \omega) = v(P, T) \left[ 1 - \left( 2Q_{\mu}^{-1}(P, T, \omega) / \tan(\pi a/2) \right) \right]$ , using a temperature dependent  $Q$ -model,  $Q_{\mu}(P, T, \omega) = A\omega^a \exp[a(H^* + PV^*)/RT]$ , where we set the exponent  $a = 0.15$ , activation energy  $H^* = 500$  kJ/mol, activation volume  $V^* = 2.0 \times 10^{-5}$  m<sup>3</sup>/mol, and the amplitude  $A = 0.049$ .

### **Half-Space Cooling (HSC) Model**

The vertical temperature profile of the HSC model<sup>2-3</sup> is a simple function of age, being the solution to the one dimensional thermal diffusion equation for an infinite half-space, which takes the same form as the temperature profile in the conductive layer of the thermal model described above. In contrast with the temperature parameterization for the seismic inversion, the error-function temperature profile for the HSC model continues infinitely with depth and explicitly does not include adiabatic heating.

### **Small-Scale Convection Simulation**

## References

1. McKenzie, D.P., Some remarks on heat flow and gravity anomalies, *J. Geophys. Res.*, *72*, 6261-6273, 1967.
2. Turcotte, D.L. and E.R. Oxburgh, Finite amplitude convection cells and continental drift, *J. Fluid Mech.*, *28*, 29-42, 1967.
3. Parker, R.L. and D.W. Oldenburg, Thermal model of ocean ridges, *Nature Phys. Sci.*, *242*, 137-139, 1973.
4. Parsons, B. and J.G. Sclater, An analysis of the variation of ocean floor bathymetry and heat flow with age, *J. Geophys. Res.*, *82*, 803-827, 1977.
5. Stein, C. A. and Stein, S., A model for the global variation in oceanic depth and heat flow with lithospheric age, *Nature*, *359*, 123-129, 1992.
6. Nagihara, S., C.R.B. Lister, and J.G. Sclater, Reheating of old oceanic lithosphere: Deductions from observations, *Earth Planet. Sci. Letts.*, *139*, 91-104, 1996.
7. Richter, F. M. and B. Parsons On the interaction of two scales of convection in the mantle, *J. Geophys. Res.*, *80*, 2529-2541, 1975.
8. Parsons, B. and McKenzie, D., Mantle convection and thermal structure of the plates, *J. Geophys. Res.*, *83*, 4485-4496, 1978.
9. Davaille, A. and C. Jaupart, Onset of thermal convection in fluids with temperature-dependent viscosity: application to the oceanic lithosphere, *J. Geophys. Res.*, *99*, 19,853-19,866, 1994.
10. Houseman, G. and D.P. McKenzie, Numerical experiments on the onset of convective instability in the Earth's mantle, *Geophys. J. R. Astron. Soc.*, *68*, 133-164, 1982.
11. Crough, S.T., Thermal origin of mid-plate hot-spot swells, *Geophys. J. R. Astron. Soc.*, *55*, 451-470, 1978.
12. McNutt, M.K., Superswells, *Revs. Geophys.*, *36*, 211-244, 1998.
13. Romanowicz, B. and Y. Gung, Superplumes from the core-mantle boundary to the lithosphere: Implications for heat flux, *Science*, *296*, 513-516, 2002.
14. Le Douaran, S. and B. Parsons, A note on the correction of ocean floor depths for sediment loading, *J. Geophys. Res.*, *87*, 4715-4722, 1982.
15. Schroeder, W., The empirical age-depth relation and depth anomalies in the Pacific Ocean, *J. Geophys. Res.*, *89*, 9873-9884, 1984.
16. Coffin, M.F., and O. Eldholm, Large igneous provinces: crustal structure, dimensions, and external consequences, *Revs. Geophys.*, *32*, 1-36, 1994.
17. White, R.S., D. McKenzie, and R.K. O'Nions, Oceanic crustal thickness measurements and rare earth element inversions, *J. Geophys. Res.*, *97*, 19,683-19,715, 1992.

18. Nishimura, C.E. and D.W. Forsyth, The anisotropic structure of the upper mantle in the Pacific, *Geophys. J.*, *96*, 203-229, 1989.
19. Ekström, G. & Dziewonski, A.M., The unique anisotropy of the Pacific upper mantle, *Nature*, *394*, 168-172, 1998.
20. Zhang, Y.-S. and T. Lay, Evolution of oceanic upper mantle structure, *Phys. Earth Planet. Ints*, *114*, 71-80, 1999.
21. Goes, S., Govers, R., and Vacher, R., Shallow mantle temperatures under Europe from P and S wave tomography, *J. Geophys. Res.*, *105*, 11,153-11,169, 2000.
22. Shapiro, N.M. and M.H. Ritzwoller, Monte-Carlo inversion for a global shear velocity model of the crust and upper mantle, *Geophys. J. Int.*, *51*, 88-105, 2002.
23. Shapiro, N.M. and M.H. Ritzwoller, Thermodynamic constraints on seismic inversions, *Geophys. J. Int.*, submitted, 2003.
24. Ritzwoller, M.H. and A.L. Levshin, Eurasian surface wave tomography: Group velocities, *J. Geophys. Res.*, *103*, 4839 - 4878 1998.
25. Trampert, J. & Woodhouse, J.H., Global phase velocity maps of Love and Rayleigh waves between 40 and 150 s period, *Geophys. J. Int.**122*, 675-690, 1995.
26. Ritzwoller, M.H., N.M. Shapiro, M.P. Barmin, and A.L. Levshin, Global surface wave diffraction tomography, *J. Geophys. Res.*, *107(B12)*, 233, 2003.
27. McDonough, W.F. & R.L. Rudnick, Mineralogy and composition of the upper mantle, in: *Ultrahigh-pressure mineralogy: physics and chemistry of the Earth's deep interior*, R.J. Hemley, Editor, 139-164, Mineralogical Society of America, Washington, DC, 1998.
28. Sobolev, S.V. et al., Upper mantle temperatures from teleseismic tomography of French Massif Central including effects of composition, mineral reactions, anharmonicity, anelasticity and partial melt. *Earth Planet. Sci. Letts.*, *157*, 193-207, 1996.
29. Mueller, R.D., W.R. Roest, J.-Y. Royer, L.M. Gahagan, and J.G. Sclater, Digital isochrons of the world's ocean floor, *J. Geophys. Res.*, *102*, 3211-3214, 1997.

**Acknowledgments.** The data used in this work were obtained from the IRIS Data Management Center and the GEOSCOPE Data Center. The authors are grateful to researchers at Harvard and Utrecht Universities for contributing phase velocity measurements to this study. We thank Anatoli Levshin, William Landuyt, Rosa Bernal, Liz Zea, and Abir van Hunen for help in preparing the data set. Aspects of this work were supported by the US National Science Foundation and the Packard Foundation.

**Supplementary information** accompanies the paper at: [http://ciei.colorado.edu/pubs/2003/7\\_suppl.pdf](http://ciei.colorado.edu/pubs/2003/7_suppl.pdf)

**Competing interests statement.** The authors declare that they have no competing financial interests.

**Correspondence** and requests for materials should be addressed to M.H.R. ([ritzwoller@ciei.colorado.edu](mailto:ritzwoller@ciei.colorado.edu)).

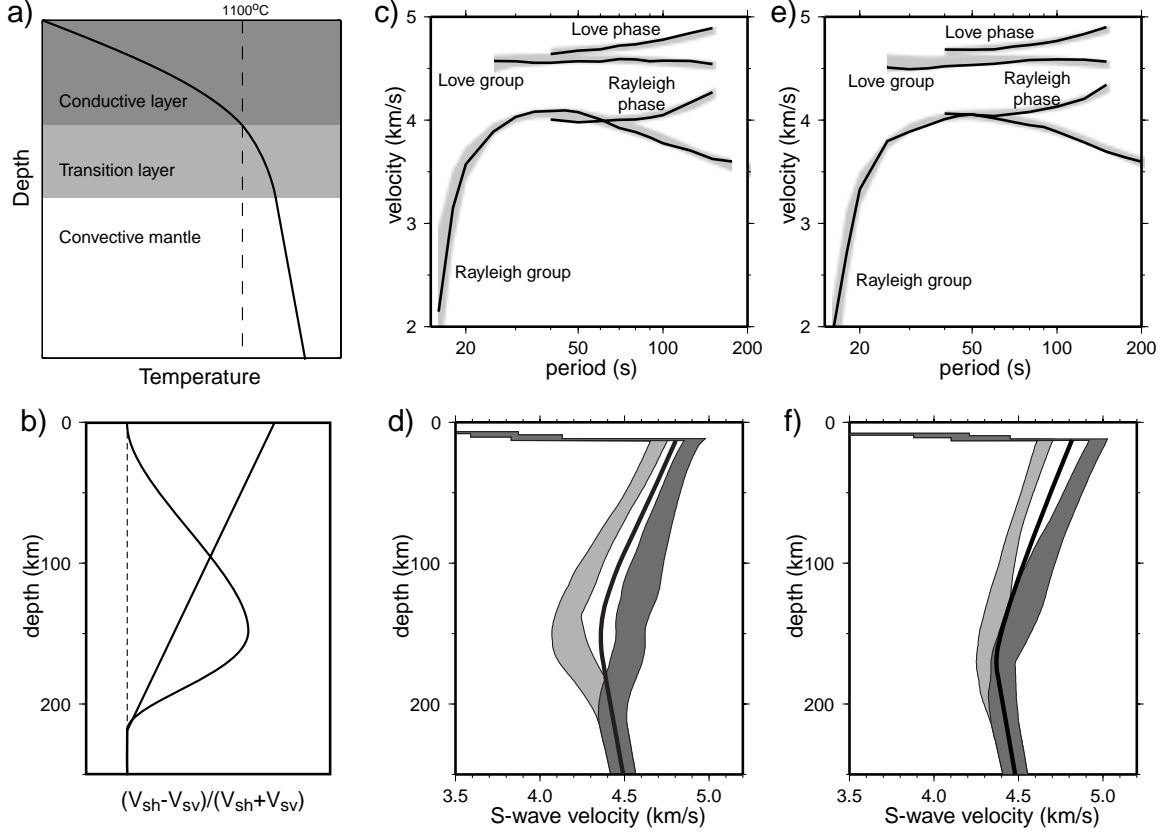
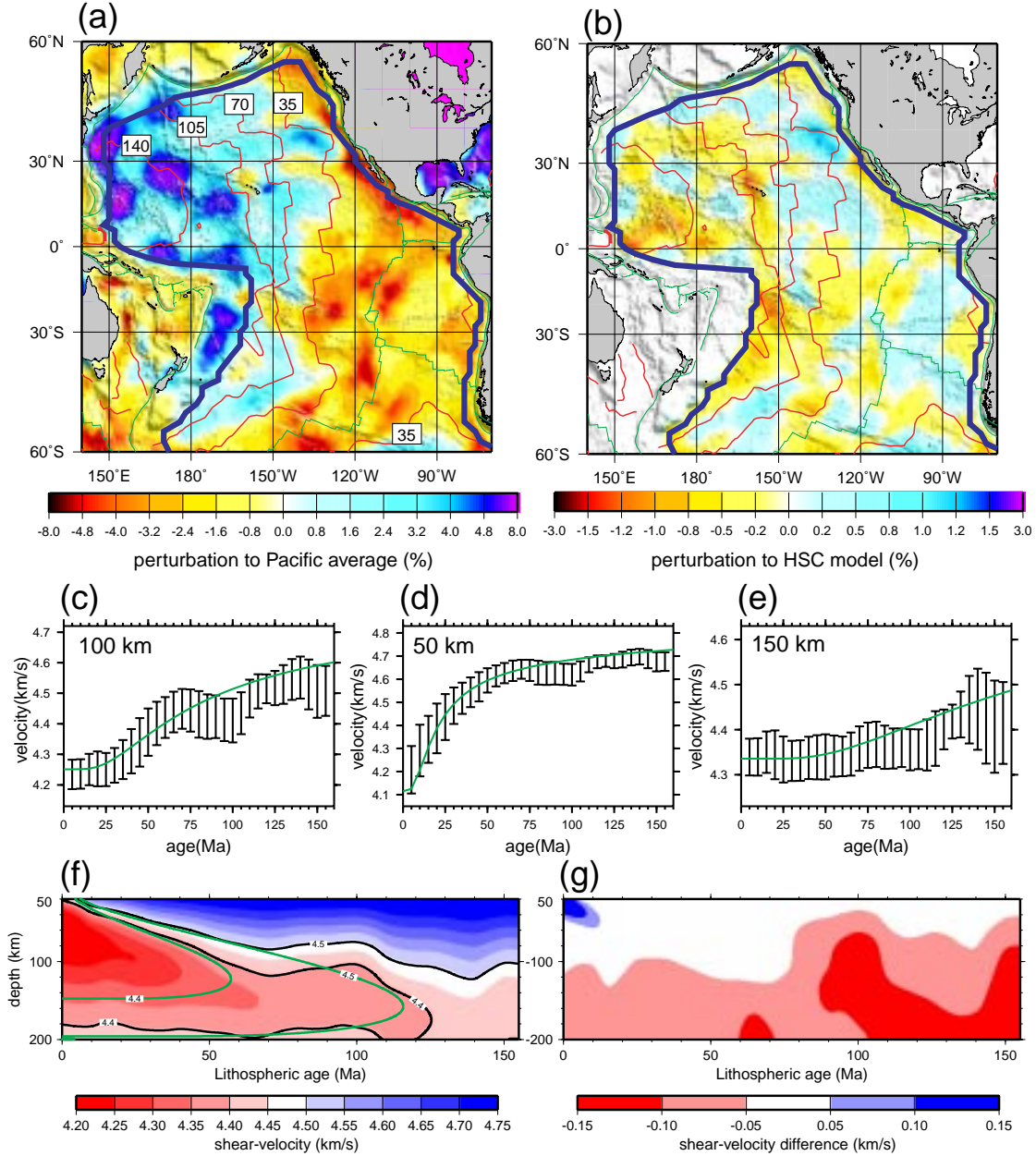


Figure 1: **Thermal parameterization and inversion at two points in the Pacific.** (a) The thermal parameterization is defined by an error function that represent temperatures in the lithosphere underlain by an adiabatic gradient in the convective mantle (asthenosphere), joined smoothly by a transition region. The two unknowns are the “apparent thermal age” of the lithosphere and the “potential temperature” of the asthenosphere. (b) Radial anisotropy is introduced as a combination of the two basis functions shown here. (c) - (d) Inversion results for a point in the Central Pacific (14°N, 200°E). Predictions from the ensemble of acceptable models (grey lines) to the four observed dispersion curves (black lines) are shown in (c). The ensemble of acceptable models is shown in (d), where the light grey-shaded envelope is  $V_{sv}$  and the dark grey-shaded envelope is  $V_{sh}$ . The solid line is median of the ensemble of isotropic shear velocities,  $V_s$ , which derive directly from the thermal model. (e) - (f) Inversion results for a point in the Western Pacific (42°N, 160°E).



**Figure 2: Shear velocity structure of the Pacific upper mantle and trend with lithospheric age.**

(a) Isotropic shear velocity,  $V_s$ , at 100 km depth, as a perturbation to the average at this depth across the Pacific (4.362 km/sec). The green lines denote plate boundaries, the red lines are isochrons of lithospheric age in Ma, and the blue contour encloses the region where there are lithospheric age estimates<sup>29</sup>. (b)  $V_s$  at 100 km depth presented as a perturbation to the prediction from the HSC model. (c) - (e) Shear velocity, averaged in 5 Ma lithospheric age bins across the Pacific, is plotted versus lithospheric age at 100 km, 50 km, and 150 km depth. Error bars represent the standard deviation within each age range. The continuous green lines are the predictions from the HSC model. (f)  $V_s$  averaged across the Pacific plotted versus lithospheric age. The green lines are isotachs (lines of constant shear velocity) from the HSC model. (g) Difference between the Pacific average  $V_s$  and the prediction from the HSC model. Reds identify areas where the observed  $V_s$  is slower than the HSC model predicts.

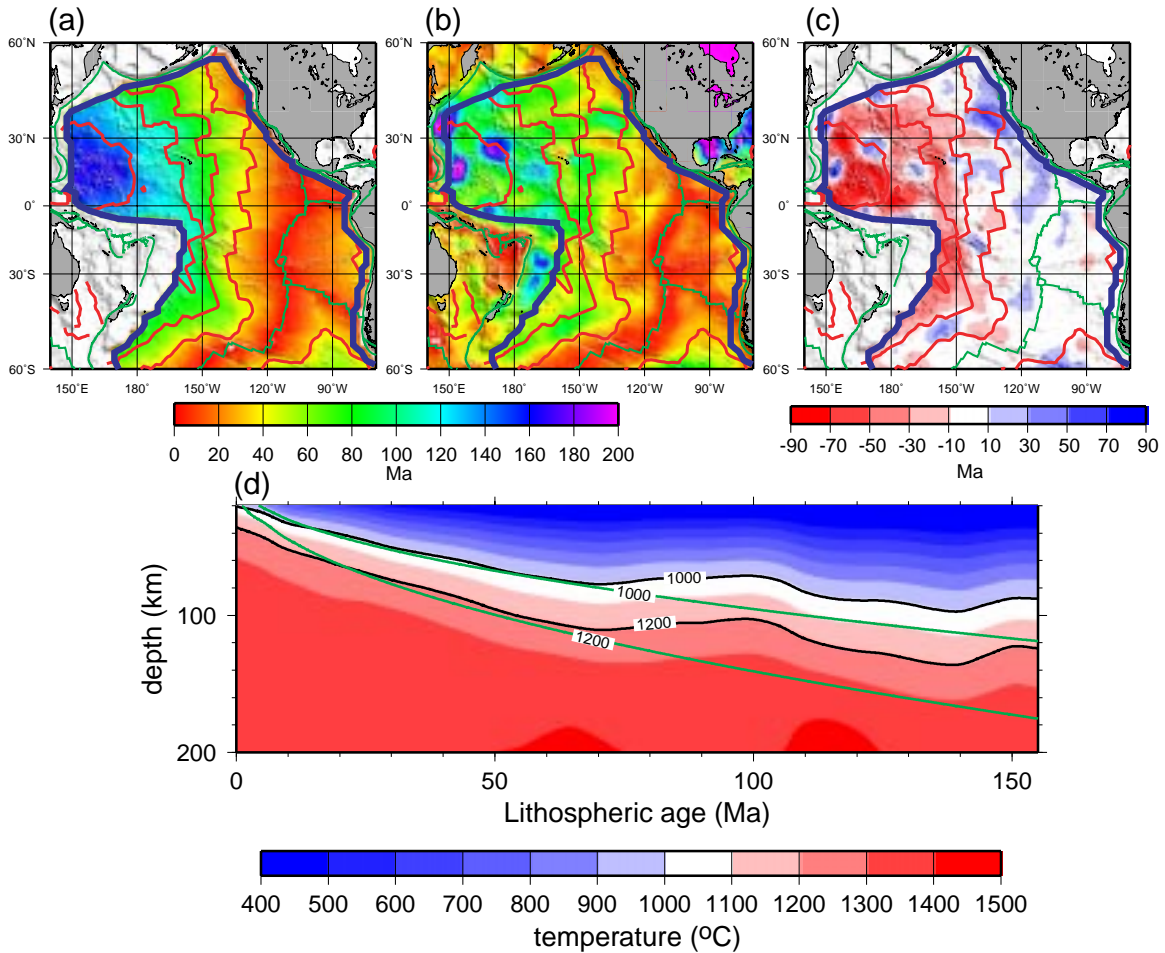


Figure 3: **Thermal structure of the Pacific upper mantle and trend with lithospheric age.** (a) Lithospheric age in Ma, presented as a reference<sup>29</sup>. (b) Apparent thermal age,  $\tau$ . (c) Difference between the lithospheric age and the apparent thermal age. Reds denote that the apparent thermal age is younger than the lithospheric age. In (a) - (c), the green, red, and blue lines are as in Figure 2a,b. (d) Upper mantle temperature averaged across the Pacific plotted versus lithospheric age. The green lines are isotherms from the HSC model.

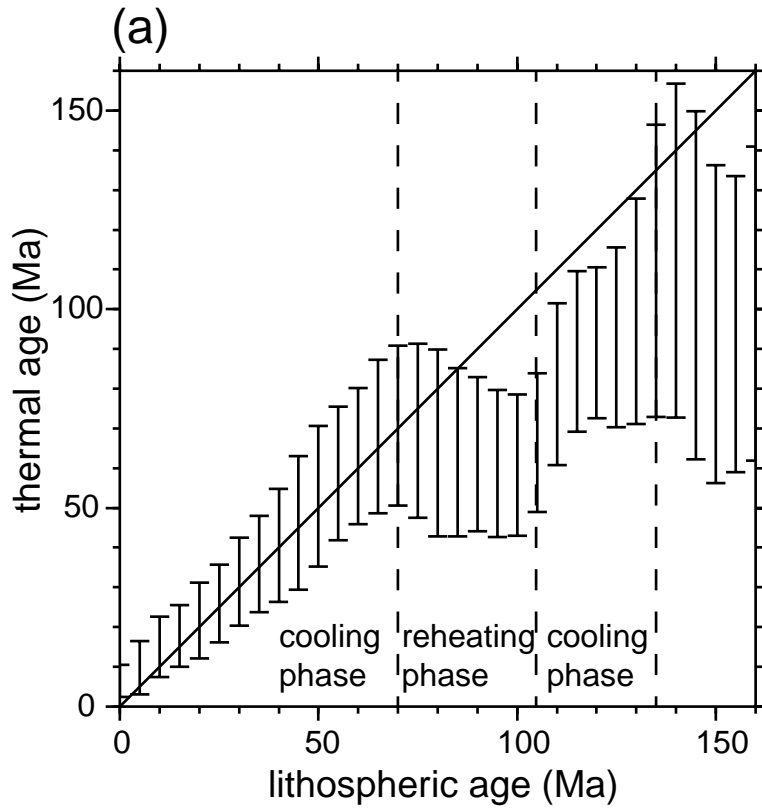


Figure 4: (a) Comparison between apparent thermal age,  $\tau$ , and lithospheric age. Apparent thermal age is averaged in 5 Ma lithospheric age bins across the Pacific and error bars represent the standard deviation within each age range. Two phases of average lithospheric cooling are identified, 0-70 Ma and 100 - 135 Ma, bracketing a phase of in which the Pacific lithosphere undergoes reheating, on average.